Ca^{2+} release via IP_3Rs increases RyR mediated Ca^{2+} spark frequency in ventricular cardiomyocytes without altering spark amplitude and duration

Agnė Tilūnaitė[1,4], David Ladd[1,4,5], Hilary Hunt[1,4], Christian Soeller[3], H. Llewelyn Roderick[2], Edmund J. Crampin[1,5,†], Vijay Rajagopal[4,†,*]

1 Systems Biology Laboratory, School of Mathematics and Statistics, University of Melbourne, Australia
2 Laboratory of Experimental Cardiology, Department of Cardiovascular Sciences, KU Leuven, Leuven, Belgium
3 Living Systems Institute, University of Exeter, Exeter EX4 4QD, UK
4 Cell Structure and Mechanobiology Group, Department of Biomedical Engineering, Melbourne School of Engineering, University of Melbourne, Australia
5 ARC Centre of Excellence in Convergent Bio-Nano Science and Technology, School of Chemical and Biomedical Engineering, University of Melbourne, Australia

† These authors contributed equally to the supervision of this work.
* Corresponding author
Email: vijay.rajagopal@unimelb.edu.au

Abstract

Calcium plays critical roles in cardiac cells, coupling electrical excitation to mechanical contraction with each heartbeat, while simultaneously mediating biochemical signals that regulate cell growth. While ryanodine receptors (RyRs) are fundamental to generation of elementary calcium release events (sparks) and global calcium elevations that underlie excitation-contraction coupling (ECC), calcium release via inositol 1,4,5-trisphosphate receptors (IP_3Rs) is also reported in cardiomyocytes. IP_3R calcium release modifies ECC as well as contributing to downstream regulation of hypertrophic gene expression. Recent studies suggest that proximal localisation of IP_3Rs with RyRs contributes to their ability to modify Ca^{2+} handling during ECC. Here we aim to determine the mechanism by which IP_3Rs modify Ca^{2+} handling in cardiomyocytes. We develop a mathematical model incorporating the stochastic behaviour of receptor opening that allows for the parametric tuning of the system to reveal the impact of IP_3Rs on spark activation. By testing multiple spark initiation mechanisms, we find that Ca^{2+} release via IP_3Rs result in increased propensity for spark initiation within the cardiac dyad. Our simulations suggest that opening of IP_3Rs elevates Ca^{2+} within the dyad, which increase the probability of spark initiation. Finally, we find that while increasing the number of IP_3Rs increases the probability of spark formation, it has little effect on spark amplitude, duration, or overall shape. Our study therefore suggests that IP_3R play a critical role in modulating Ca^{2+} signaling for excitation contraction coupling

Author summary

While Ca^{2+} release through ryanodine receptors (RyRs) initiates contraction in cardiomyocytes, the role of inositol 1,4,5-trisphosphate receptors (IP_3Rs) in

cardiomyocytes is less clear with Ca^{2+} release through these channels being invoked in regulating ECC and hypertrophic signalling. RyRs generate cytosolic Ca^{2+} signals through elemental Ca^{2+} release events called sparks. The mechanisms by which IP_3Rs influence cytosolic Ca^{2+} are not well understood. We created a 1D model of calcium spark formation in a cardiomyocyte dyad—the primary site of elemental RyR-based calcium release. We investigated possible behaviours of IP_3Rs and their interaction with RyRs in generating Ca^{2+} sparks. We show that for high IP_3 concentration, a large number of IP_3Rs and high IP_3R affinity are required to noticeably affect spark shape. At lower IP_3 concentration IP_3Rs can increase Ca^{2+} spark activity, but do not significantly alter the spark shape. Finally our simulations suggest that spark frequency can be reliably increased when IP_3Rsactivity is such that a small continuous Ca^{2+} flux is introduced to the dyad to elevate Ca^{2+} , and not via brief but high Ca^{2+} release from these receptors.

Introduction

Calcium plays a fundamentally important role in the regulation of each heartbeat. Ca^{2+} flux through L-type Ca^{2+} channels (LTCC) couples electrical activation to muscle contraction through excitation-contraction coupling (ECC) [1, 2]. Membrane depolarisation triggers a small influx of calcium through voltage-gated LTCCs (Fig. 1A) into 10-15 nm wide calcium microdomains [3, 4] called dyads. In these regions, LTCC channels are juxtaposed with a set of Ca^{2+} channels called ryanodine receptors (RyRs) on the intracellular sarcoplasmic reticulum (SR) compartment. RyRs are sensitised by the Ca^{2+} influx and release a larger amount of Ca^{2+} from the SR. This local Ca^{2+} release event at the dyad is known as a calcium spark (Fig. 1B) and cardiac contraction is determined by the sum of these elementary local Ca^{2+} release events at the many dyads regularly distributed through the cardiomyocyte volume.

In a majority of cell types, neurohormonal stimulation of intracellular Ca^{2+} is mediated by inositol 1,4,5-trisphosphate (IP_3) and IP_3 receptors (IP_3Rs) located on the endoplasmic reticulum (ER) [5]. In cardiomyocytes, activation of G-protein coupled receptors (GPCR) for neurotransmitters such as endothelin-1 (ET-1) and angiotensin-II (AngII) leads to elevation of IP_3 and Ca^{2+} release via IP_3Rs [6–9]. Crosstalk between IP_3Rs and RyRs, in which activation of IP_3Rs via elevated IP_3 leads to recruitment of neighbouring RyRs receptors, leading to larger Ca^{2+} release, was first suggested in smooth muscle cells [10]. Similar interaction between IP_3Rs and RyRs has also been proposed in embryonic myocytes [11, 12], atrial cardiac myocytes [13–15], spontaneously hypertensive rat (SHR) myocytes [8], and rabbit ventricular myocytes [16]. Given the lower abundance and Ca^{2+} flux of IP_3Rs relative to RyRs, how they can affect ECC remains poorly understood. In particular, the characteristics of IP_3R gating that may lead to recruitment of RyR receptors also remains to be determined.

Experimental investigations [17] and computational models [18, 19] of Ca^{2+} sparks have elucidated the role of the spatial distribution and density of RyR channels, and their stochastic interactions, in determining the spatio-temporal characteristics of Ca^{2+} sparks in health and disease [20]. IP_3Rs are proposed to collocate with RyRs [8, 16, 21–23] and are also known to exhibit increased expression in pathological conditions [24], here we use computational modelling to test a hypothesis that IP_3R Ca^{2+} release modulates Ca^{2+} spark activity, and thereby affects cytosolic Ca^{2+} and ECC.

Previously, stochastic and deterministic models have been developed which investigate the properties of RyRs in generating Ca^{2+} sparks [18, 25–30]. Computational models of IP_3Rs have also been developed primarily for various cell types where IP_3Rs are the predominant intracellular Ca^{2+} release channel [31–35]. Deterministic temporal

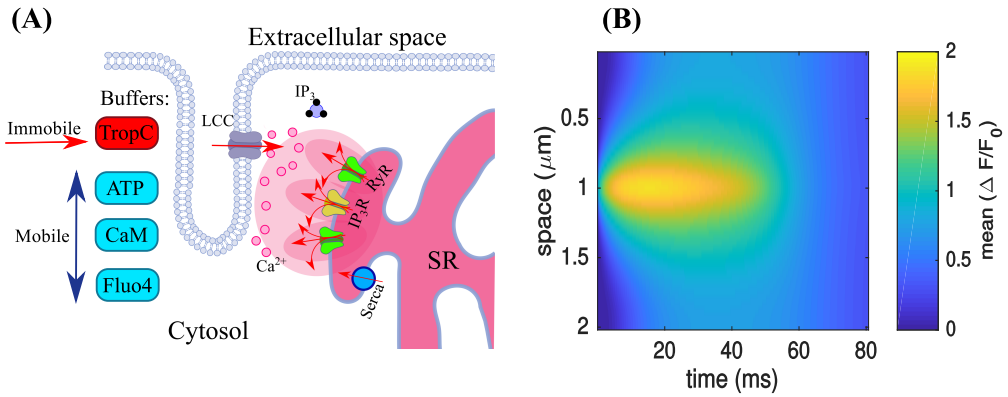

Fig 1. Schematic illustrations of the key components at the dyadic junction underlying calcium sparks: (A) elements of Ca^{2+} signalling in a dyad and (B) illustration of an average Ca^{2+} spark.

models have been proposed that include both IP_3Rs and RyRs, but do not provide information about sparks or spatial interactions between these two SR Ca^{2+} release channels [36, 37]. To date, the role of IP_3Rs in Ca^{2+} spark formation, including both RyR and IP_3Rs in a stochastic computational model, has not been investigated.

In this study, we investigate the influence that IP_3R activation may have in the shape and temporal behavior of Ca^{2+} sparks through stochastic interaction between IP_3Rs and RyRs. We creates a 1D spatial model of cardiomyocyte dyads containing stochastically opening RyR and IP_3Rs. Using this model, we examine how Ca^{2+} -mediated interaction (crosstalk) between IP_3R and RyR channels impacts the spatio-temporal profile of the Ca^{2+} spark. We investigate the sensitivity of spark initiation and shape to a range of IP_3R gating parameters and IP_3 concentration. Our findings suggest that for low IP_3 concentrations, Ca^{2+} release via IP_3Rs is insufficient to initiate sparks but they increase the probability of spark events without changing spark shape. The model also suggests that a small sustained Ca^{2+} flux from active IP_3Rs diffusing to neighbouring RyRs can trigger spark formation.

Materials and methods

Model formulation

We model the transport of Ca^{2+} as a reaction-diffusion system that describes the movement of Ca^{2+} in three compartments: cytosolic (Ca_c); junctional sarcoplasmic reticulum (Ca_{JSR}); and network sarcoplasmic reticulum (Ca_{NSR}):

$$\frac{\partial[Ca_c]}{\partial t} = D_c\nabla^2[Ca_c] + J_{buff} - J_{SERCA} + J_{release} \quad (1)$$

$$\frac{\partial[Ca_{JSR}]}{\partial t} = \beta_{JSR}(-J_{release} + J_{refill}) \quad (2)$$

$$\frac{\partial[Ca_{NSR}]}{\partial t} = D_{NSR}\nabla^2[Ca_{NSR}] + J_{SERCA} - J_{refill}, \quad (3)$$

where D_c and D_{NSR} represent the Ca^{2+} diffusivities in the cytosol and the network SR respectively (the junctional SR is assumed to be a small and hence well-mixed volume). β_{JSR} represents the calsequestrin buffer, which is modelled following the approach of Keizer *et al.* [38]. J_{SERCA} represents the flux of Ca^{2+} from the cytosol into the NSR through the sarco-endoplasmic reticular Ca^{2+}-ATPase (SERCA) pumps. J_{refill}

represents the flux of Ca^{2+} refilling the JSR compartment from the NSR. J_{buff} is the flux of Ca^{2+} as it binds and unbinds to buffers in the cytosol. J_{release} represents the flux of Ca^{2+} from the JSR into the cytosol through RyRs and IP_3Rs , and is defined such that

$$J_{\text{release}} = (g_{\text{RyR}} \cdot \text{RyR}_{\text{open}} + g_{\text{IP}_3\text{R}} \cdot \text{IP}_3\text{R}_{\text{open}}) \cdot (\text{Ca}_{\text{JSR}} - \text{Ca}_c), \tag{4}$$

where RyR_{open} and $\text{IP}_3\text{R}_{\text{open}}$ represent the number of open RyRs and IP_3Rs, respectively. RyR_{open} is calculated using a re-scaled stochastic model as proposed by Cannell *et al.* [18]. $\text{IP3R}_{\text{open}}$ is calculated based on the stochastic two-state 'park-drive' model proposed by Siekmann *et al.* [34] based on fitting single channel data [39, 40], as implemented by Cao *et al.* [35]. g_{RyR}, $g_{\text{IP}_3\text{R}}$ represent RyR and IP_3R flux coefficients. A schematic illustration of these compartments and fluxes is provided in Fig. 2A. For simplicity, the effect of LTCCs in triggering receptor opening in the dyad was implemented by directly opening 30 RyRs, rather than introducing additional Ca^{2+} via LTCCs in each cycle. J_{buff} is the Ca^{2+} flux on binding to mobile and immobile cytosolic Ca^{2+} buffers. The transport of Ca^{2+} bound to mobile buffers (B^m) including adenosine trisphosphate (ATP), the calcium indicator Fluo4, and calmodulin, and Ca^{2+} binding to the immobile buffer Troponin C, (B^{im}), are included as:

$$\frac{\partial [B^m]}{\partial t} = D_{B_m} \nabla^2 [B^m] + k^m_{\text{on}} [B^m][\text{Ca}] - k^m_{\text{off}} [\text{CaB}^m] \tag{5}$$

$$\frac{\partial [B^{im}]}{\partial t} = k^{im}_{\text{on}} [B^{im}][\text{Ca}] - k^{im}_{\text{off}} [\text{CaB}^{im}], \tag{6}$$

where k^m_{on} and k^m_{off} represent the on and off rates for mobile buffers (ATP, CaM or Fluo4), and k^{im}_{on} and k^{im}_{off} are the on and off rate for the immobile buffer (TnC). Further expressions and model details may be found in the Supplementary Text S1.

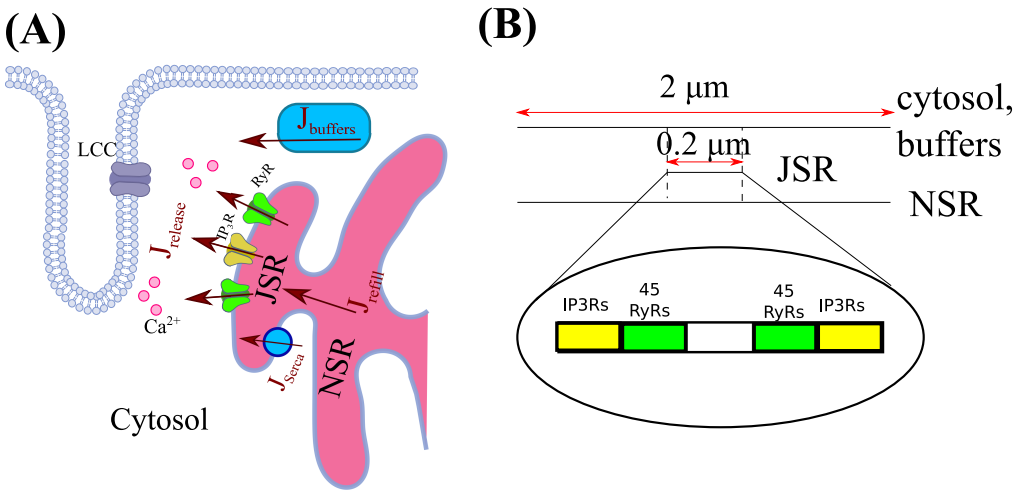

Fig 2. Diagram of 1D model settings: (A) Model fluxes and compartments, (B) Spatial settings of the dyad. SERCA is positioned outside JSR location.

Numerical implementation

We simulated the reaction-diffusion system and stochastic interactions between RyR and IP_3Rs within a single dyad on a 1D geometry to reflect the experimental line-scan recording of calcium sparks and transients. This reduced-order representation enabled an investigation into the influence of IP_3Rs on Ca^{2+} spark generation in the dyad. This

choice of representation was further justified by previous detailed 3D simulations of Ca^{2+} spark generation, which showed that the spatial distribution of RyRs on the dyad was not critical to the spark profile when the number of RyRs in the cluster was greater than 9 [41].

The spatial settings for each cell compartment and receptors along this 1D geometry are illustrated in Fig. 2B. The 0.2 μm-wide dyad has 45 RyRs positioned on either side of the midline, separated by 0.04 μm, with a variable number of IP_3Rs placed another 0.04 μm from the centre at both ends of the dyad.

The partial differential equations (PDEs) were discretized in space using a finite difference scheme. The resulting system of ODEs was solved using a first-order Runge-Kutta method with a maximum time step $dt = 1 \times 10^{-4}$ ms and a spatial step $dx = 0.04$ μm. Stochastic IP_3R and RyR gating states were solved using a hybrid Gillespie method. All software was written using Matlab2017b (The MathWorks Inc., Natick, Massachusetts).

Results

We tested the sensitivity of the Ca^{2+} spark profile to interactions between IP_3Rs and RyRs by comparing sparks with no IP_3Rs to sparks generated with different numbers of IP_3Rs and varying parameter settings. Specifically, we investigated the dependence of amplitude, duration and frequency of spark events to: number of IP_3Rs; IP_3Rs Ca^{2+}-sensitivity; and IP_3 concentration.

Number of IP_3Rs per dyad does not affect the shape of LTCC-initiated Ca^{2+} sparks

To determine the effects of IP_3R-mediated Ca^{2+} release on the shape of the Ca^{2+} spark, single spark events were initiated within a dyad by opening 30 RyRs per cluster at $t = 0$ ms, with different numbers of IP_3Rs: 0, 5, 10, or 20 per cluster (yellow box, Fig. 2B). Simulations were run for $T_{obs} = 80$ ms, and each simulation was repeated 108 times. Example simulation outputs are given in Supplementary Figures 1 and 2. Representative fluorescence trace, and means and 95% confidence intervals for Ca^{2+} concentration in the JSR at the RyR locations, and IP_3Rs and RyR receptor open populations, are provided in Fig. 3. These simulation results show that LTCC-triggered sparks (Fig. 3, first column) are similar in shape and duration irrespective of the number of IP_3Rs.

Additionally, in all simulations, minimum $[Ca^{2+}]_{JSR}$ was ≈ 200 μM at ≈ 50 ms, which coincides with the time RyRs start to close. This is consistent with the hypothesis that spark termination is related to $[Ca^{2+}]_{JSR}$ depletion, as suggested previously [42, 43]. IP_3Rs were active primarily at the start of simulations (Fig. 3, third column) when only $\approx 20\%$ of IP_3Rs were open. However, RyRs fluctuated to $\approx 45\%$ of RyRs for ≈ 50 ms and closed at ≈ 60 ms (Fig. 3, fourth column). This suggests that RyRs, but not IP_3Rs , primarily determine spark shape. Since IP_3Rs are mostly active at the beginning of simulations, they may however play a role in spark initiation.

IP_3Rs can facilitate spark initiation

To test the role that IP_3Rs play in spark activation, we next considered which dyad trigger settings were sufficient to generate a spark. Experiments on cardiac and smooth muscle cells suggested that IP_3Rs may not create a spark by themselves, but can facilitate neighbouring RyR opening [10, 12, 13]. Therefore we tested how one dyad will behave when: (a) no initiation is applied; (b) 5 IP_3Rs are opened at $t = 0$ ms; (c) 5

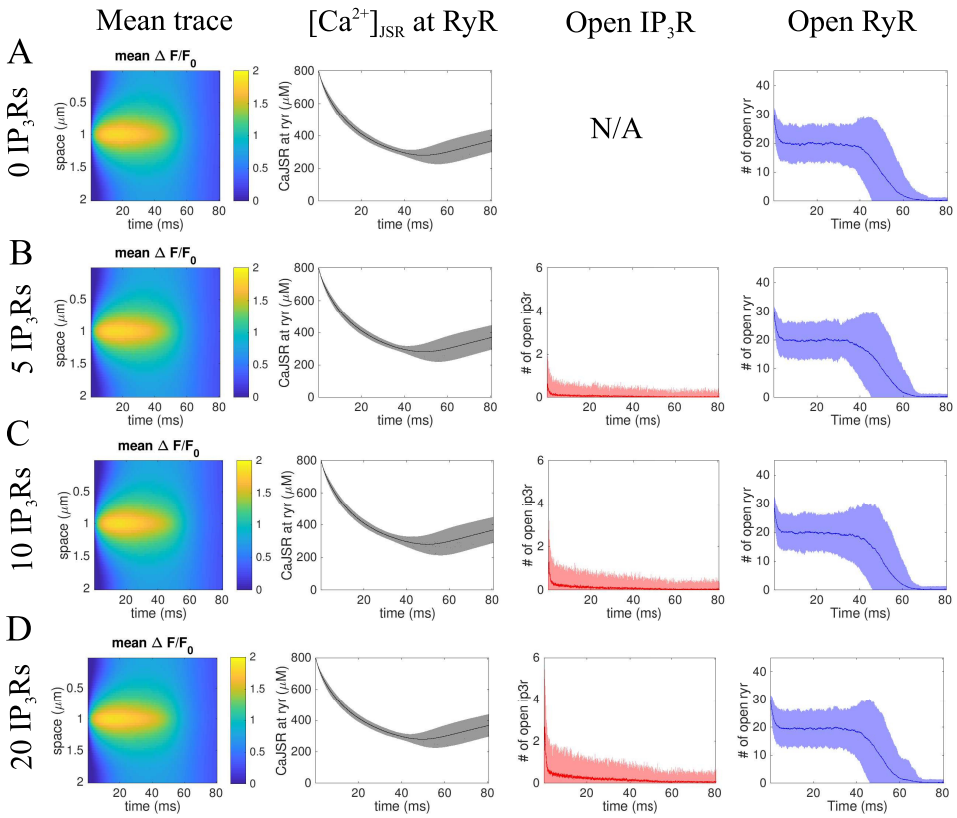

Fig 3. Initiated spark shape is not affected by number of IP_3Rs. Profiles for sparks initiated by opening RyR channels at $t = 0$ ms, with different numbers of IP_3Rs per cluster: (A) 0, (B) 5, (C) 10, (D) 20 IP_3Rs. Panels show mean and 95% confidence intervals ($\mu \pm 1.96\sigma$) from 108 simulations, from left to right: fluorescence trace, $[Ca^{2+}]_{JSR}$ at the RyR positions, number of opened IP_3Rs and number of opened RyRs.

RyRs are opened at $t = 0$ ms; (d) 5 IP_3Rs and 2 RyRs are opened at $t = 0$ ms; and (e) consistently open IP_3Rs (IP_3R "leakage").

Simulation results shown in Fig. 3 do not show significant variability in spark shape with different number of IP_3Rs , therefore we fixed the number of IP_3Rs to 20. Simulations were run for $T_{obs} = 80$ ms and repeated 108 times, for each of these 5 triggering mechanisms. We calculated the percentage of simulations which showed sparks (we assumed a spark to have occured if $\max(\Delta F/F_0) > 1$), and spark initiation times (when the maximum value of the fluorescence trace occurred) within each simulation. Results shown in Fig. 4 indicate that both the percentage of simulations that depict spark initiation (Fig. 4A) and the spark initiation times within a simulation (Fig. 4B) depend on the trigger mechanism. Simulations with (a) no trigger, (b) 5 opened IP_3Rs , and (d) mixture of opened receptors, showed sparks in only $\approx 12\%, \approx 23\%$ and $\approx 32\%$ of runs, respectively (Fig. 4A). Furthermore, the small number of sparks and the broad distribution of their time to peak (Fig. 4B) suggests that in each of these cases spark initiation occurred at a random time following channel opening. Nevertheless spark amplitudes were approximately the same in these simulations (shown in Supplementary Figure 3). These results indicate that intermittently opening IP_3Rs increases the probability of spark initiation but may not reliably initiate a spark under fixed IP_3 concentration (0.15 μM).

Simulations with (c) 5 opened RyRs and (e) leaking IP_3Rs showed spark initiation

(A)

Trigger	Percentage of simulations with detectable spark
(a) No trigger	12
(b) 5 IP_3Rs	23
(c) 5 RyRs	97
(d) 5 IP_3Rs and 2 RyRs	32
(e) Leaking IP_3R	100

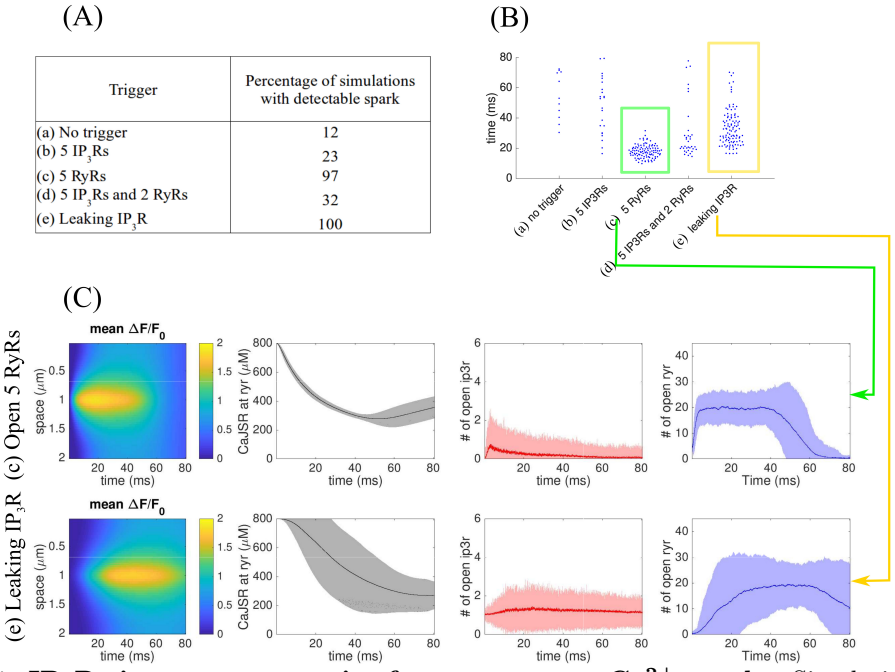

Fig 4. IP_3Rs increase propensity for spontaneous Ca^{2+} sparks. Simulation results using different triggers. (A) Percentage of 108 runs that had $\max \Delta CaF4/CaF4_0 > 1$ under different triggering mechanisms mentioned above. (B) Times when maximum values of the trace were reached. (C) Mean and 95% confidence intervals ($\mu \pm 1.96\sigma$) of simulations under 5 opened RyRs at $t = 0$ ms (top) and leaking IP_3R (bottom). Columns illustrate averaged fluorescence trace of reacted runs, Ca_{JSR} concentration at the RyR locations, number of opened IP_3Rs and number of opened RyRs (from right to left, respectively).

in almost all simulation runs. However, there was a difference in the distributions of spark initiation times (Fig. 4B): (c) 5 opened RyRs resulted in almost instantaneous spark initiation, while IP_3R "leakage" increased the frequency of sparks, but spark initiation times were distributed more widely. Fig. 4B suggests that opening RyRs (c) instantaneously initiates sparks, while highly active IP_3Rs facilitate spark formation by priming RyRs for activation thereby increasing their liklihood for spontaneous opening (e).

"Leaking" IP_3Rs showed more broadly distributed spark initiation times, indicated in the much wider confidence intervals in bottom plots of Fig. 4C. Furthermore, the time to initiation was longer compared to the opened RyR case (Fig. 4C, first column). Decay but not recovery of $[Ca^{2+}]_{JSR}$ can be seen in averaged results (second column, Fig. 4C). These observations again indicate that Ca^{2+} sparks were initiated spontaneously with IP_3R activated slow Ca^{2+} release.

IP_3R open probability influences spark shape

Cardiomyocytes express three isoforms of IP_3R: IP_3R1, IP_3R2 and IP_3R3 [21, 44, 45]. Type 2 isoform is predominant [21] and has the highest IP_3 binding affinity, followed by type 1 and type 3 being the least sensitive to IP_3. As mathematical models using the type 1 isoform are more developed, in simulations upto this point we used parameter values in the IP_3R model that had previously been fitted to single channel recordings on

type 1 IP_3 receptors [46]. To explore the influence of the Ca^{2+}-sensitivity of different IP_3R isoforms we shifted the Ca^{2+}-sensitivity curve (supplementary Figure 7) to give qualitative estimates of the different isoforms provided in the experimental literature [34, 47].

Simulations with type 2 receptor parameters and varying number of IP_3Rs are shown in Fig. 5 for $[IP_3] = 0.15$ μM. Sparks were initiated by opening 5 RyRs at $t = 0$ ms. It can be seen that, as for type 1 parameters, spark amplitudes were not affected by the number of receptors (Fig. 5A). However, unlike type 1 simulations, type 2 parameters showed an increase in spark duration under higher number of IP_3Rs (Fig. 5B). This difference may be due to type 1 parameter simulations showing the number of opened IP_3Rs to be highest at $t = 0$ ms and decreasing subsequently throughout the simulation (Fig. 3), while for type 2 parameters IP_3Rs are initially closed over the first $t = 5$ ms, and may open again subsequently during the simulation (Fig. 5C). This difference is in particular evident for simulations with 20 IP_3Rs, when type 2 parameters showed on average 1 opened IP_3R after $t = 10$ ms, while for type 1 parameters all IP_3Rs are on average closed by this point (Fig. 5D).

High $[IP_3]$ increases robustness of spark initiation

IP_3R behaviour depends on cytosolic Ca^{2+} and IP_3 concentrations [47]. Increased $[IP_3]$ overcomes Ca^{2+} dependent inhibition, which could be a factor in the dyadic environment. Therefore we next investigated spark triggering mechanisms and spark shape with 20 IP_3Rs at 6 different IP_3 concentrations ranging from 0.05 μM to 3 μM. As in previous simulations, we calculate the percentage of simulations in which a spark was initiated, as well as the spark initiation time (time to maximum of the fluorescence trace) and spark shape.

Table 1 shows the percentage of simulation runs in which a spark was initiated, for $[IP_3] = 0.05; 0.15; 0.5; 1; 2; 3$ μM. In these simulations IP_3R type 1 parameters were used, and different triggering mechanisms were considered, as in previous simulations. For "leaking" IP_3Rs as well as simulations triggered with opened RyRs, reliable spark initiation occurred for all IP_3 concentrations. For simulations triggered with IP_3R opening, the probability of succesful spark generation increased with increasing IP_3 concentration.

Trigger \ $[IP_3]$	0.05 μM	0.15 μM	0.5 μM	1 μM	2 μM	3 μM
(b) 5 open IP_3Rs	17	23	54	86	100	100
(c) 5 open RyRs	99	97	100	100	100	100
(e) Leaking IP_3Rs	99	100	100	100	100	100

Table 1. Percentage of simulations with detected sparks under different IP_3 concentration and triggering mechanisms. Percentages were calculated from 108 simulations with $T_{obs} = 80$ ms and 20 IP_3Rs. Triggering mechanism and IP_3 concentration are provided in rows and columns, respectively.

Summaries of spark shape and spark initiation times for these triggering mechanisms under different IP_3 concentrations are shown in Fig. 6. Full simulation summaries are provided in Supplementary Figures 4-6. For simulations triggered by opened RyRs, spark times are not strongly affected by IP_3 alterations, however for opened IP_3Rs and "leaking" IP_3Rs , more robust spark initiation times are observed under higher IP_3 concentration (Fig. 6A). Spark amplitudes remained similar under all IP_3 concentrations (Fig. 6B), showing only modest increase with increasing $[IP_3]$. These

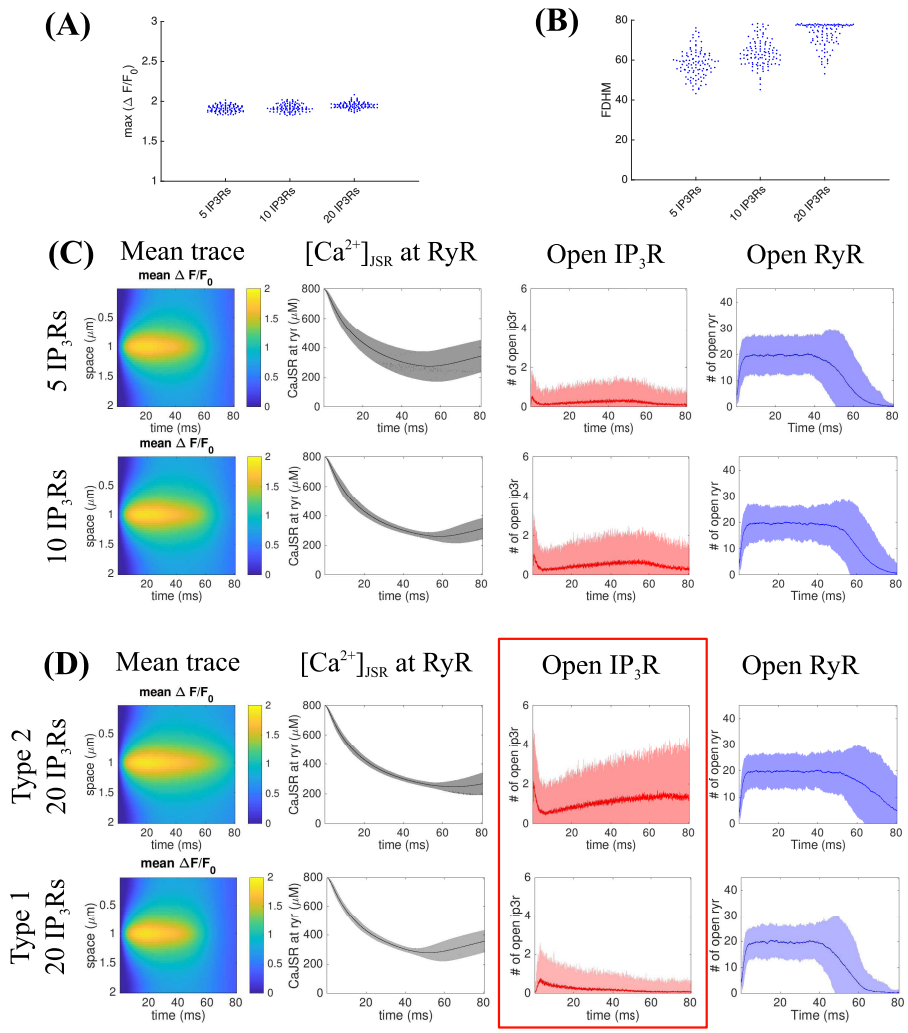

Fig 5. The number of IP_3Rs can alter spark duration in type 2 receptors. Summaries of 108 simulations using varying numbers of IP_3Rs . (A) Spark amplitudes, (B) spark duration, (C) Simulation summaries (means and 95% confidence intervals) under 5 and 10 IP_3Rs per cluster. From left to right: fluorescence trace, $[Ca^{2+}]_{JSR}$ at the RyR positions, number of opened IP_3Rs and number of opened RyRs. $[IP_3]$ was set to 0.15 μM. (D) Comparison of type 2 and type 1 IP_3Rs simulations under 20 IP_3Rs per cluster and $[IP_3] = 0.15$ μM. RyR receptors were forcefully opened at $t = 0$. Spark duration is increased by type 2 IP_3Rs but not type 1.

observations confirm that for IP_3R type 1 parameters, spark properties are determined predominantly by RyR activity.

Finally, we compared simulations for type 1 and type 2 parameter sets at different $[IP_3]$, shown in Fig. 7. A more detailed summary of effect of different $[IP_3]$ on spark shape and initiation times in simulations with type 2 parameter set are provided in Supplementary Figure 8. As illustrated by the third column of Fig. 7, IP_3R activity increases with higher $[IP_3]$ under both parameter sets. For type 1 parameters, IP_3Rs showed highest activity at $t \approx 5$ ms after which receptors within the cluster started to close, while for type 2 parameters IP_3Rs were continuously open under higher $[IP_3]$. This difference influences RyR behaviour and hence spark duration (red boxes in Fig. 7).

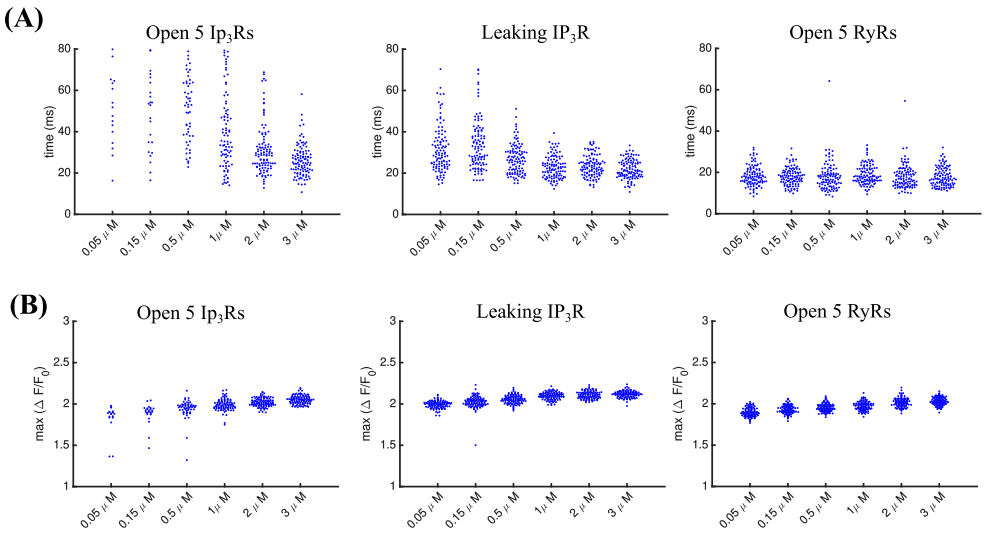

Fig 6. Increasing [IP$_3$] makes spark initiation more robust. 108 simulations summaries using different [IP$_3$]. (A) Times when maximum values of the trace were reached; (B) Spark amplitudes. Full simulation summaries are provided in Supplementary Figures 4-6. All simulations were run for $T_{obs} = 80$ ms and 20 IP$_3$Rs.

Discussion

IP$_3$Rs are expressed in cardiomyocytes, where they colocalise with RyRs in dyads, yet a functional role in Ca^{2+} spark formation – elementary Ca^{2+} events underlying cardiac ECC – is unclear, in part because of the dominance of RyR Ca^{2+} release. In this study, we have sought to determine the potential for IP$_3$R Ca^{2+} release to contribute to spark formation in the cardiomyocyte dyad. We developed a 1D spatial model accounting for stochastic RyR and IP$_3$R gating and examined spark initiation in a single dyad. Specifically, we investigated whether IP$_3$Rs in a dyad can affect spark initiation and shape and how this changes depending on modelled IP$_3$R gating behaviour.

Model assumptions and their implications

In our model we made two major assumptions: 1) SR receptors are in close proximity to each other, but they do not overlap, and 2) there is no Ca^{2+} diffusion in the JSR compartment. If receptors overlap, then Ca^{2+} depletion in the JSR could occur more quickly due to the larger Ca^{2+} flux through the SR receptors. This overlap could subsequently cause spark termination and reduce spark duration. Ca^{2+} diffusion in the JSR may also change spark duration by affecting Ca^{2+} depletion in the SR. However Cannell et al. [18] showed that the physical distribution of RyRs within the dyad will not greatly affect the spark profile in clusters greater than 9 RyRs. Walker et al. [48] also showed that the propensity of spark formation from stochastic release of Ca^{2+} from ion channels increased with larger and denser clusters of RyRs. Furthermore, our study shows that IP$_3$R activation also does not alter spark profile.

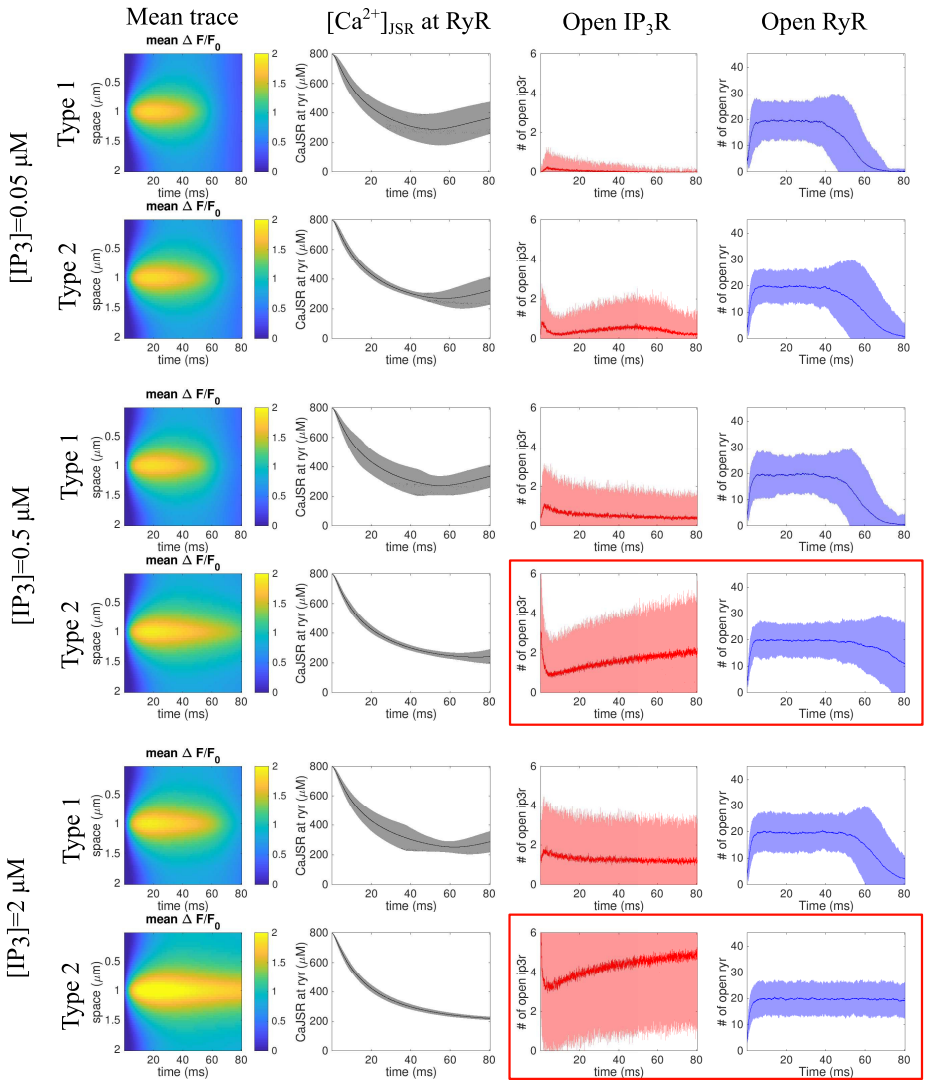

Fig 7. Comparison of type 1 and type 2 parameter simulations under varying [IP$_3$]. Mean and 95% confidence intervals ($\mu \pm 1.96\sigma$) of simulations under type 1 (top) and type 2 (bottom) parameter sets. Columns illustrate averaged fluorescence trace of reacted runs, Ca_{JSR} concentration at the RyR locations, number of opened IP$_3$Rs and number of opened RyRs (from right to left, respectively). All simulations were run for $T_{obs} = 80$ ms and with 20 IP$_3$Rs.

Our simulations support the idea that Ca^{2+} via IP$_3$R prime RyRs for ECC in disease.

Our results indicate that for type 1 IP$_3$R , the number of IP$_3$Rs in a cluster does not significantly affect spark shape when triggered by the L-type channel Ca^{2+} flux. This implies that, in healthy cardiac cells, sparks are insensitive to the relatively small perturbations caused by IP$_3$R opening. However, IP$_3$R expression increases significantly in diseased cardiomyocytes [8, 44]. Increasing numbers of IP$_3$Rs and in particular 'leaky' IP$_3$Rs , as would result from increased diastolic Ca^{2+} concentration, lead to increased spark initiation frequency. This suggests that the increase in IP$_3$R expression could be a compensatory mechanism to dyad uncoupling from electrical activity in disease [49].

In the absence of Ca^{2+} influx through the LTCC, however, our analysis indicated that prolonged IP_3R "leakage" was able to initiate a spontaneous spark, while intermittently opening IP_3Rs were not sufficient to reliably trigger a spark (figure 4A). These results agree with a range of experiments in cardiac cells [10, 12, 13] reporting that opened IP_3Rs do not provide sufficient Ca^{2+} to trigger an event, however their activation can sensitize neighbouring RyR clusters. In hypertrophic rat cardiomyocytes and in atrial cells, IP_3R channels have been been shown to increase diastolic $[Ca^{2+}]$ [50]. Our simulations imply that this rise in diastolic $[Ca^{2+}]$ can directly cause the increase in spontaneous calcium transients that is also observed in hypertrophic cells [50, 51].

"Leaky" IP_3R in our simulations represented a type of spark trigger where IP_3R channels were constitutively open. While ion channels do not physiologically remain constiutively open it is plausible that the "leak" may represent the elevation in Ca^{2+} arising from several intermittently opening and closing IP_3Rs during ECC.

Our simulations indicate that increasing $[IP_3]$ can make spark initiation more robust and also slightly increase spark duration (Fig. 6). However, spark amplitudes remained similar under investigated $[IP_3]$ (Fig. 6B). Specifically, our simulations agree with previous findings in mouse and rabbit ventricular myocytes [16, 51] which found no significant changes in amplitude immediately after addition of 10 μM IP_3. However, Domeier et al. [16] indicated that the amplitude of the sparks may change in longer duration experiments (after $\approx 7min$ following IP_3 application). The authors also suggested that IP_3 application did not affect spark duration, while our simulations generated slightly longer sparks under 2 μM IP_3 compared to 0.05 μM IP_3 concentration. It should be noted that Domeier et al. [16] used imaging resolution of 3 ms per scan, while in our simulations the time resolution was set to 0.0001 ms.

The potential roles of different isoforms of IP_3R

We based our IP_3R model on the Siekmann et al. stochastic two-state park-drive model [35, 46] to simulate IP_3R induced calcium release. This model was parametrised for type 1 IP_3Rs with the Ca^{2+} sensitivity ranging between 0.1 μ.M and 10 μM (see Supplementary Figure 7). This sensitivity was measured in type I IP_3R channels expressed in COS cells [**?**]. To investigate type 2 IP_3R behaviour, we altered model parameters to qualitatively represent Ca^{2+}-sensitivity curve as provided in [34, 47]. The type 2 IP_3Rs are sensitive to Ca^{2+} in the range 0.01 μM to 1 μM (see Supplementary Figure 7).

Our simulations suggest that type-2 IP_3Rs would alter the shape of the Ca^{2+} spark by releasing Ca^{2+} at the early rise phase as well as the late decay phase of the spark timeline. While this is surprising, given the wide range of Ca^{2+} sensitivities reported [**?**] even for one IP_3R isoform type in experiments, it is unclear what the specific parameters for IP_3Rs for Ca^{2+} sensitivity should be. In addition, the 1D dyadic simulations here do not include structural details that have been shown to produce Ca^{2+} concentrations within the dyad of 6 - 10 μM [52, 53]. Therefore, both types of IP_3Rs may actually be inhibited by a high concentration of calcium within the dyad during Ca^{2+} spark events. This would mean that neither IP_3R isoform would affect spark shape but the sensitising effect would remain. Additionally, IP_3 sensitivity is suggested to vary between isoforms [**?**]. Further work needs to be done to incorporate more spatial detail of the collocation of IP_3Rs and RyRs as well as the isoform differences to further test the validity of our type 2 isoform predictions in this study.

Conclusion

IP_3Rs may not affect spark initiation or shape in healthy cells with coupled RyRs and LTCC. In the absence of LTCC trigger, however, we tested 5 different initiation cases and showed that Ca^{2+} release via IP_3R can trigger sparks by sensitizing neighbouring RyR clusters.

Further work is needed in order to link these findings on IP_3Rs-influenced spark formation to models of IP_3 signalling in cardiomyocytes [54, 55], and multi-scale integration of stochastic spark formation to understand how this impacts on global cytosolic Ca^{2+} transient dynamics and excitation-contraction coupling under normal and disease conditions [56, 57].

Supporting information

S1 Text: Model equations, parameters and references.

S2 Figures: Supplementary figures for single dyad simulations.

Acknowledgments

This research was supported in part by the Australian Government through the Australian Research Council Discovery Projects funding scheme (project DP170101358) to EJC and VR, and the Australian Research Council Centre of Excellence in Convergent Bio-Nano Science and Technology (project CE140100036) to EJC. HLR wishes to acknowledge financial support from the Research Foundation Flanders (FWO) through Project Grant G08861N and Odysseus programme Grant 90663.

References

1. Fearnley CJ, Roderick HL, Bootman MD. Calcium signaling in cardiac myocytes. Cold Spring Harbor Perspectives in Biology. 2011;3(11):a004242.

2. Berridge MJ. The Inositol Trisphosphate/Calcium Signaling Pathway in Health and Disease. Physiological Reviews. 2016;96(4):1261–1296.

3. Gilbert G, Demydenko K, Dries E, Puertas RD, Jin X, Sipido K, et al. Calcium Signaling in Cardiomyocyte Function. Cold Spring Harbor Perspectives in Biology. 2020;12:a035428.

4. Langer G, Peskoff A. Calcium concentration and movement in the diadic cleft space of the cardiac ventricular cell. Biophysical Journal. 1996;70(3):1169–1182.

5. Camors E, Valdivia HH. CaMKII regulation of cardiac ryanodine receptors and inositol triphosphate receptors. Frontiers in Pharmacology. 2014;5:101.

6. Drawnel FM, Archer CR, Roderick HL. The role of the paracrine/autocrine mediator endothelin-1 in regulation of cardiac contractility and growth. British Journal of Pharmacology. 2013;168(2):296–317. doi:10.1111/j.1476-5381.2012.02195.x.

7. Nakayama H, Bodi I, Maillet M, DeSantiago J, Domeier TL, Mikoshiba K, et al. The IP3 receptor regulates cardiac hypertrophy in response to select stimuli. Circulation Research. 2010;107(5):659–666.

8. Harzheim D, Movassagh M, Foo RSY, Ritter O, Tashfeen A, Conway SJ, et al. Increased InsP3Rs in the junctional sarcoplasmic reticulum augment Ca2+ transients and arrhythmias associated with cardiac hypertrophy. Proceedings of the National Academy of Sciences. 2009;106(27):11406–11411.

9. Cooling MT, Hunter PJ, Crampin EJ. Sensitivity of NFAT cycling to cytosolic calcium concentration: implications for hypertrophic signals in cardiac myocytes. Biophysical Journal. 2009;96(6):2095–2104.

10. Gordienko D, Bolton T. Crosstalk between ryanodine receptors and IP3 receptors as a factor shaping spontaneous Ca2+-release events in rabbit portal vein myocytes. The Journal of Physiology. 2002;542(3):743–762.

11. Sasse P, Zhang J, Cleemann L, Morad M, Hescheler J, Fleischmann BK. Intracellular Ca2+ oscillations, a potential pacemaking mechanism in early embryonic heart cells. The Journal of General Physiology. 2007;130(2):133–144.

12. Rapila R, Korhonen T, Tavi P. Excitation–contraction coupling of the mouse embryonic cardiomyocyte. The Journal of General Physiology. 2008;132(4):397–405.

13. Horn T, Ullrich ND, Egger M. 'Eventless' InsP3-dependent SR-Ca2+ release affecting atrial Ca2+ sparks. The Journal of Physiology. 2013;591(8):2103–2111.

14. Wullschleger M, Blanch J, Egger M. Functional local crosstalk of inositol 1, 4, 5-trisphosphate receptor-and ryanodine receptor-dependent Ca2+ release in atrial cardiomyocytes. Cardiovascular Research. 2017;113(5):542–552.

15. Zima AV, Blatter LA. Inositol-1,4,5-trisphosphate-dependent Ca2+ signalling in cat atrial excitation–contraction coupling and arrhythmias. The Journal of Physiology. 2004;555(3):607–615. doi:10.1113/jphysiol.2003.058529.

16. Domeier TL, Zima AV, Maxwell JT, Huke S, Mignery GA, Blatter LA. IP3 receptor-dependent Ca2+ release modulates excitation-contraction coupling in rabbit ventricular myocytes. American Journal of Physiology-Heart and Circulatory Physiology. 2008;294(2):H596–H604.

17. Galice S, Xie Y, Yang Y, Sato D, Bers DM. Size matters: ryanodine receptor cluster size affects arrhythmogenic sarcoplasmic reticulum Calcium Release. Journal of the American Heart Association. 2018;7(13).

18. Cannell MB, Kong CHT, Imtiaz MS, Laver DR. Control of sarcoplasmic reticulum Ca2+release by stochastic RyR gating within a 3D model of the cardiac dyad and importance of induction decay for CICR termination. Biophysical Journal. 2013;104(10):2149–2159.

19. Xie Y, Yang Y, Galice S, Bers DM, Sato D. Size Matters : Ryanodine Receptor Cluster Size Heterogeneity Potentiates Calcium Waves. Biophysical Journal. 2019;116(3):530–539.

20. Kolstad TR, van den Brink J, MacQuaide N, Lunde PK, Frisk M, Aronsen JM, et al. Ryanodine receptor dispersion disrupts Ca^{2+} release in failing cardiac myocytes. eLife. 2018;7:e39427.

21. Lipp P, Laine M, Tovey SC, Burrell KM, Berridge MJ, Li W, et al. Functional InsP3 receptors that may modulate excitation–contraction coupling in the heart. Current Biology. 2000;10(15):939 – S1.

22. Hund TJ, Ziman AP, Lederer W, Mohler PJ. The cardiac IP3 receptor: uncovering the role of "the other" calcium-release channel. Journal of Molecular and Cellular Cardiology. 2008;45(2):159–161.

23. Bare D, Kettlun C, Liang M, Bers D, Mignery G. Cardiac type 2 inositol 1,4,5-trisphosphate receptor: Interaction and modulation by calcium/calmodulin-dependent protein kinase II. Journal of Biological Chemistry. 2005;280(16):15912–15920.

24. Harzheim D, Talasila A, Movassagh M, Foo R, Figg N, Bootman M, et al. Elevated InsP3R expression underlies enhanced calcium fluxes and spontaneous extra-cystolic calcium release events in hypertropic cardiac myocytes. Channels. 2010;4(1):1–5.

25. Stern MD, Song LS, Cheng H, Sham JS, Yang HT, Boheler KR, et al. Local Control Models of Cardiac Excitation–Contraction Coupling: A Possible Role for Allosteric Interactions between Ryanodine Receptors. The Journal of General Physiology. 1999;113(3):469.

26. Sobie EA, Dilly KW, dos Santos Cruz J, Lederer WJ, Jafri MS. Termination of cardiac Ca2+ sparks: an investigative mathematical model of calcium-induced calcium release. Biophysical Journal. 2002;83(1):59–78.

27. Walker MA, Williams GSB, Kohl T, Lehnart SE, Jafri MS, Greenstein JL, et al. Superresolution Modeling of Calcium Release in the Heart. Biophysical Journal. 2014;107(12):3018–3029.

28. Vierheller J, Neubert W, Falcke M, Gilbert S, Nagaiah C. A multiscale computational model of spatially resolved calcium cycling in cardiac myocytes: From detailed cleft dynamics to the whole cell concentration profiles. Frontiers in Physiology. 2015;6.

29. Soeller C, Cannell MB. Estimation of the sarcoplasmic reticulum Ca2+ release flux underlying Ca2+ sparks. Biophysical Journal. 2002;82(5):2396–2414. doi:10.1016/S0006-3495(02)75584-7.

30. Rajagopal V, Bass G, Walker CG, Crossman DJ, Petzer A, Hickey A, et al. Examination of the Effects of Heterogeneous Organization of RyR Clusters, Myofibrils and Mitochondria on Ca2+ Release Patterns in Cardiomyocytes. PLOS Computational Biology. 2015;11(9):1–31.

31. Marchant JS, Parker I. Role of elementary Ca2+ puffs in generating repetitive Ca2+ oscillations. The EMBO Journal. 2001;20(1-2):65–76.

32. Thurley K, Tovey SC, Moenke G, Prince VL, Meena A, Thomas AP, et al. Reliable encoding of stimulus intensities within random sequences of intracellular Ca2+ spikes. Sci Signal. 2014;7(331):ra59–ra59.

33. Dupont G, Abou-Lovergne A, Combettes L. Stochastic aspects of oscillatory Ca2+ dynamics in hepatocytes. Biophysical Journal. 2008;95(5):2193–2202.

34. Siekmann I, Wagner II LE, Yule D, Crampin EJ, Sneyd J. A kinetic model for type I and II IP3R accounting for mode changes. Biophysical Journal. 2012;103(4):658–668.

35. Cao P, Tan X, Donovan G, Sanderson MJ, Sneyd J. A Deterministic Model Predicts the Properties of Stochastic Calcium Oscillations in Airway Smooth Muscle Cells. PLoS Computational Biology. 2014;10(8).

36. Johny JP, Plank MJ, David T. Importance of altered levels of SERCA, IP3R, and RyR in vascular smooth muscle cell. Biophysical Journal. 2017;112(2):265–287.

37. Hunt H, Tilunaite A, Bass G, Soeller C, Roderick HL, Rajagopal V, et al. IP3R Ca2+ release shapes the cytosolic Ca2+ transient for hypertrophic signalling in cardiomyocytes. Biophysical Journal. 2020;.

38. Keizer J, Levine L. Ryanodine receptor adaptation and Ca2+ (-) induced Ca2+ release-dependent Ca2+ oscillations. Biophysical Journal. 1996;71(6):3477–3487.

39. Siekmann I, Wagner II LE, Yule D, Fox C, Bryant D, Crampin EJ, et al. MCMC estimation of markov models for ion channels. Biophysical Journal. 2011;100(8):1919–1929.

40. Siekmann I, Sneyd J, Crampin EJ. MCMC can detect nonidentifiable models. Biophysical Journal. 2012;103(11):2275–2286.

41. Cannell MB, Kong CHT, Imtiaz MS, Laver DR. Control of Sarcoplasmic Reticulum Ca2+ Release by Stochastic RyR Gating within a 3D Model of the Cardiac Dyad and Importance of Induction Decay for CICR Termination. Biophysical Journal. 2013;104(10):2149–2159.

42. Zima AV, Picht E, Bers DM, Blatter LA. Termination of cardiac Ca^{2+} sparks. Circulation Research. 2008;103(8):e105–e115.

43. Stern MD, Cheng H. Putting out the fire: what terminates calcium-induced calcium release in cardiac muscle? Cell Calcium. 2004;35(6):591–601.

44. Signore S, Sorrentino A, Ferreira-Martins J, Kannappan R, Shafaie M, Del Ben F, et al. Inositol 1, 4, 5-trisphosphate receptors and human left ventricular myocytes. Circulation. 2013;128(12):1286–1297.

45. Perez PJ, Ramos-Franco J, Fill M, Mignery GA. Identification and functional reconstitution of the type 2 inositol 1, 4, 5-trisphosphate receptor from ventricular cardiac myocytes. Journal of Biological Chemistry. 1997;272(38):23961–23969.

46. Siekmann I, Wagner II LE, Yule D, Crampin EJ, Sneyd J. A kinetic model for type I and II IP3R accounting for mode changes. Biophysical Journal. 2012;103(4):658–668.

47. Wagner II LE, Yule DI. Differential regulation of the InsP3 receptor type-1 and-2 single channel properties by InsP3, Ca2+ and ATP. The Journal of Physiology. 2012;590(14):3245–3259.

48. Walker MA, Williams GSB, Kohl T, Lehnart SE, Jafri MS, Greenstein JL, et al. Superresolution Modeling of Calcium Release in the Heart. Biophysical Journal. 2014;107(12):3018–3029.

49. Garcia MI, Boehning D. Cardiac inositol 1, 4, 5-trisphosphate receptors. Biochimica et Biophysica Acta. 2017;1864(6):907–914.

50. Harzheim D, Movassagh M, Foo RSY, Ritter O, Tashfeen A, Conway SJ, et al. Increased InsP(3)Rs in the junctional sarcoplasmic reticulum augment Ca2+ transients and arrhythmias associated with cardiac hypertrophy. Proceedings of the National Academy of Sciences. 2009;106(27):11406–11411.

51. Blanch i Salvador J, Egger M. Obstruction of ventricular Ca 2+-dependent arrhythmogenicity by inositol 1,4,5-trisphosphate-triggered sarcoplasmic reticulum Ca 2+release. The Journal of Physiology. 2018;596(18):4323–4340.

52. Hake J, Edwards AG, Yu Z, Kekenes-Huskey PM, Michailova AP, McCammon JA, et al. Modelling cardiac calcium sparks in a three-dimensional reconstruction of a calcium release unit. The Journal of Physiology. 2012;590(18):4403–4422.

53. Rajagopal V, Bass G, Walker CG, Crossman DJ, Petzer A, Hickey A, et al. Examination of the effects of heterogeneous organization of RYR clusters, myofibrils and mitochondria on Ca2+ release patterns in cardiomyocytes. PLoS Computational Biology. 2015;11(9):e1004417–31.

54. Cooling M, Hunter P, Crampin EJ. Modeling hypertrophic IP3 transients in the cardiac myocyte. Biophysical Journal. 2007;93(10):3421–3433.

55. Cooling MT, Hunter PJ, Crampin EJ. Modelling biological modularity with CellML. Systems Biology, IET. 2008;2(2):73–79.

56. Crampin EJ, Smith NP, Hunter PJ. Multi-scale modelling and the IUPS physiome project. Journal of Molecular Histology. 2004;35(7):707–714.

57. Terkildsen JR, Niederer S, Crampin EJ, Hunter PJ, Smith NP. Using Physiome standards to couple cellular functions for rat cardiac excitation-contraction. Experimental Physiology. 2008;93(7):919–929.